



Aerosol-assisted deposition of surfactant-templated mesoporous silica membranes on porous ceramic supports

G. Xomeritakis^a, C.M. Braunbarth^a, B. Smarsly^a, N. Liu^a, R. Köhn^a,
Z. Klipowicz^b, C.J. Brinker^{a,c,*}

^a NSF Center for Microengineered Materials, The University of New Mexico, Albuquerque, NM 87131, USA

^b Department of Ceramic Engineering, Clemson University, Clemson, SC 29634, USA

^c Sandia National Laboratories, Advanced Materials Laboratory, 1001 University Blvd. SE, Suite 100, Albuquerque, NM 87106, USA

Received 23 May 2003; received in revised form 22 August 2003; accepted 25 August 2003

Abstract

We present a new approach for rapid formation of mesoporous, surfactant-templated silica membranes on coarse-pore α -Al₂O₃ ceramic supports. A surfactant-silica sol is dispersed in the gas phase in the form of small droplets and delivered to the surface of the planar support by a N₂ carrier stream. Coalescence of deposited sol droplets combined with solvent evaporation-induced self-assembly of liquid crystalline mesophases results in the formation of continuous, mesostructured silica-surfactant layers covering the surface of the support. These mesostructured silica membranes are impermeable right after synthesis and exhibit N₂ permeance in the range 10⁻⁷–10⁻⁶ mol m⁻² s⁻¹ Pa⁻¹ after surfactant removal. SEM studies revealed the presence of relatively smooth layers of thickness \sim 1 μ m on the surface of the ceramic supports while SAXS and TEM investigations revealed that these membranes possess cubic-ordered mesopores of size \sim 20 Å, without preferential orientation with respect to the substrate. Such membranes may find application in ultrafiltration separation processes, since surfactant-templating can be used for accurate control of the pore size/distribution in the proper range for a desired separation.

© 2003 Elsevier Inc. All rights reserved.

Keywords: Aerosol; Mesoporous silica; Surfactant; Membrane; Ultrafiltration

1. Introduction

The sol–gel process is a well-established route for the synthesis of a variety of porous inorganic

membranes with high thermal and chemical stability, controlled microstructure, and pore size spanning the micro- and mesoporous range. The most common sol–gel derived porous inorganic membranes are commercially available ultrafiltration membranes of composition γ -Al₂O₃, TiO₂ and ZrO₂ [1]. The precursors of these membranes are usually colloidal sols of nanometer-sized metal oxide particles, formed by hydrolysis and condensation of respective metallorganic precursors in aqueous media. Membrane formation typically

* Corresponding author. Address: NSF Center for Microengineered Materials, The University of New Mexico, Albuquerque, NM 87131, USA. Tel.: +1-505-272-7627; fax: +1-505-272-7336.

E-mail address: cjbrink@sandia.gov (C.J. Brinker).

involves sol deposition on a suitable macroporous support (e.g. α - Al_2O_3), followed by calcination to form a thin layer of closely packed, uniformly sized particles with interparticle pores of size related to the size of the primary particles [2].

These nanocrystalline ultrafiltration ceramic membranes, although commercially available for over a decade [3], may exhibit some disadvantages, e.g. reduced stability due to grain growth or phase transformations induced by high temperature heat treatments [4], and difficulties in pore size control due to corresponding difficulties in controlling the size and/or shape of the primary particles in the precursor colloidal sols.

More recently, the discovery by Mobil researchers [5] of a new class of mesoporous inorganic molecular sieves based on supramolecular surfactant templating, has suggested new opportunities for expanding the family of mesoporous inorganic membranes beyond the traditional particulate ceramic membranes described above. Mesoporous inorganic membranes (typically silica-based) made by surfactant templating approaches can exhibit improved structural stability (e.g. no grain growth or phase transformations), well-controlled pore size and pore order (dictated by the choice of surfactant template and synthesis conditions), very high surface areas and chemically tunable pore walls. For these reasons, several groups have already reported on their efforts to develop mesoporous silica membranes using evaporation-induced self assembly [6], hydrothermal treatment [7–9] or flow field induced growth [10] on a variety of non-porous or porous supports.

Our group recently demonstrated rapid formation of mesoporous silica films on planar supports by combining traditional sol–gel chemistry and surfactant self-assembly [11]. In this process, we begin with an ethanol-based, polymeric silica sol mixed with a suitable surfactant at a concentration well below the *critical micelle concentration*. During dip-coating of the support in the surfactant-silica sol, preferential evaporation of ethanol concentrates the entrained sol in non-volatile surfactant and silica species. The progressively increasing surfactant concentration drives self-assembly of silica/surfactant micelles and their

further organization into liquid crystalline mesophases, resulting in rapid formation of highly ordered mesostructured silica films with controlled pore structure (e.g. hexagonal or cubic), depending on the choice of surfactant and initial ethanol/silica/surfactant molar ratio in the starting sol. We refer to this process as evaporation-induced self-assembly (EISA).

The above dip-coating process has proven useful for formation of mesoporous films on relatively smooth supports such as non-porous Si wafers [11], or fine-pore γ - Al_2O_3 (pore size 40 Å, [12]), but cannot guarantee film formation on coarse-pore supports such as α - Al_2O_3 with pore size >100 nm. Such coarse-pore supports however, are particularly attractive as supports for gas or liquid separations since they combine low cost with reduced permeation resistance compared to multilayer ceramic supports with a final γ - Al_2O_3 top-layer. A thin mesoporous silica membrane with sharp pore size distribution coated directly on such supports could find application in ultrafiltration of large biomolecules, or serve as a support for a microporous membrane useful for gas or vapor separations [12–14]. The objective of the present paper is to demonstrate a novel and rapid method for developing mesoporous silica-based inorganic membranes by combining aerosol-assisted deposition and EISA of surfactant-templated silica sols on planar coarse-pore ceramic supports.

2. Experimental

2.1. Porous supports

The supports used for silica membrane deposition were homemade α - Al_2O_3 disks of thickness 2 mm, diameter 22 mm and pore size ~ 0.2 μm . The supports were made by pressing a commercial α - Al_2O_3 powder (Baikowski, CR-6, [15]) into green disks with a 3/8 in. dye and a hydraulic press (Carver), followed by calcination for 6 h at 1200 °C. Subsequently, one surface of the disks was polished with abrasive SiC paper (Buehler, grit size no. 320) to obtain a smooth surface for subsequent membrane deposition.

2.2. Sol preparation

The surfactant-silica sol used for membrane deposition was prepared by adding proper amounts of tetraethoxysilane (TEOS), Brij-56, a non-ionic surfactant with molecular formula $C_{16}H_{33}(OCH_2CH_2)_nOH$, $n \sim 10$, and HCl 0.07 N, to 50 g of deionized water. The composition of the silica sol on a molar basis was: $SiO_2:HCl:Brij-56:H_2O = 1:6 \times 10^{-3}:0.14:120$. Both TEOS and Brij-56 were purchased from Aldrich and were used without any further purification. The mixture was sonicated for at least 60 min to allow for complete hydrolysis of TEOS and dissolution of the surfactant. After a clear solution was obtained, the sol was aged for 2–3 h at room temperature before deposition experiments were performed.

2.3. Membrane deposition

The membrane deposition experiments were carried out using the experimental setup shown in Fig. 1. Aerosol generation was achieved using an ultrasonic humidifier (Sunbeam model 696) which allowed nebulization of ~ 40 ml of the surfactant-silica sol contained within a vertical pyrex tube of 1.75 in. OD and 6 in. high. The bottom of the pyrex tube was epoxy-sealed with a rubber band that acted as a vibrating diaphragm, transmitting the pulsation of the humidifier to the overlying surfactant-silica sol. The airborne sol droplets generated in this way were carried upwards by a N_2 carrier stream ($150 \text{ cm}^3/\text{min}$) towards a support disk suspended above the aerosol generator and surrounded by a glass funnel and a transparent plastic film. In this way, the aerosol stream bypassing the support disk around its circumference, formed an aerosol cloud above the disk where the largest aerosol droplets settled gravitationally on its top surface, resulting in film formation after drying and self-assembly. The cylindrical plastic film shown in Fig. 1 served to protect the aerosol cloud from air currents in the fume-hood where the entire setup was located.

The deposition process was typically carried out in 5-min intervals and enough time (15–20 min) was allowed between two deposition cycles in order to ensure complete evaporation of the sol-

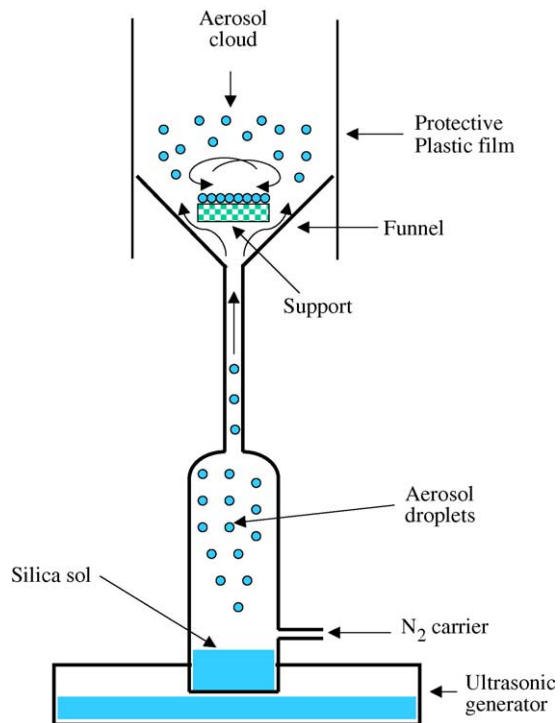


Fig. 1. Schematic representation of the experimental setup used for aerosol-assisted deposition of surfactant-templated silica membranes on coarse-pore $\alpha\text{-Al}_2\text{O}_3$ ceramic supports.

vent before resuming deposition. After deposition, the membranes were dried overnight at 120°C in a vacuum oven in order to promote silica condensation around the surfactant micelles and strengthen the microstructure. Subsequently, surfactant removal was carried out by either firing the membranes for 1 h at 400°C in air, or by extraction in a 1 N HCl solution in ethanol for 12 h at 80°C under autothermal conditions. The second method was generally preferred in order to avoid crack formation on the membrane layer induced by the large mismatch between the thermal expansion coefficient of the ceramic support and the silica membrane.

2.4. Gas permeation

The gas permeation properties of the silica membranes were determined with the experimental setup shown in Fig. 2. The membrane disks were sealed inside a custom-made stainless steel

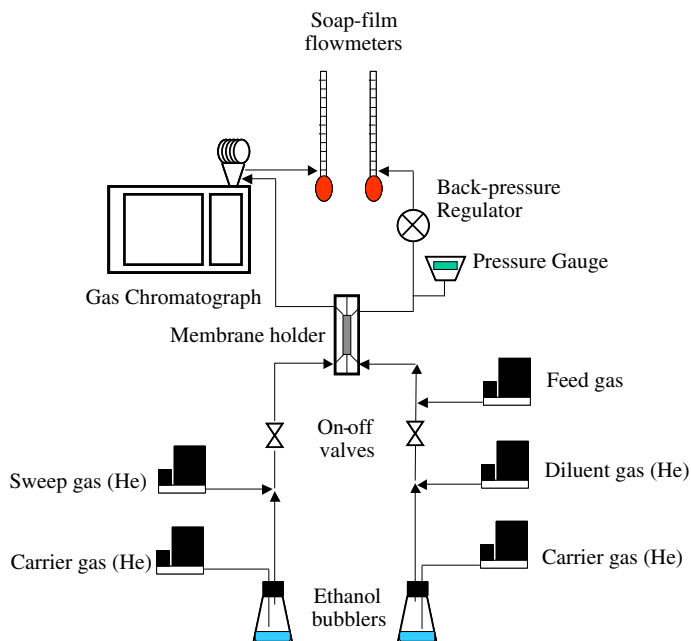


Fig. 2. Schematic representation of the experimental setup used for measurement of the gas transport properties of the supported mesoporous membranes.

permeation cell using elastomer O-rings. One side of the disk with the silica layer was flushed with a pure gas stream (e.g. He, CH₄, N₂, Ar, CO₂, SF₆) at a pressure 50–100 kPa above ambient, and the flow rate of the permeate stream exiting the other side of the holder was measured with a calibrated bubble flowmeter. For membranes with very low permeance (e.g. before surfactant removal), permeation measurements were conducted in the counter-current Wicke-Kallenbach mode. The side of the disk with the silica membrane was flushed with a pure feed gas stream (e.g. N₂), while the opposite side was flushed with a pure He sweep gas stream which was directed to a HP 5890 Gas Chromatograph for online composition analysis. The same configuration was employed to measure gas permeation in the presence of a condensable vapor, here ethanol.

2.5. Microscopy

Microscopical observations of membrane surfaces and cross-sections were performed using a Hitachi S800 Scanning Electron Microscope op-

erated at 20 kV. TEM analysis of small amounts of calcined silica films scratched off the surface of the ceramic supports were performed on a JEOL 2010 Transmission Electron Microscope operated at 200 kV. Both SEM and TEM images were acquired with a Gatan slow scan CCD camera.

2.6. XRD and GISAXS

The mesostructure of the aerosol-deposited surfactant-silica films and the relative orientation of the pores with respect to the macroporous support were studied by standard X-ray diffraction, as well as small-angle X-ray scattering experiments on uncalcined films in grazing incidence geometry (GISAXS). Regular XRD scans of thin film samples were carried out in our in-house diffractometer (Siemens D500), using Ni-filtered CuK_α radiation and θ - 2θ scan mode in a reflection geometry. GISAXS experiments were carried out using the high energy synchrotron X-rays of the Advanced Photon Source (APS) facility, sector 1-BM, in Argonne National Laboratory, Argonne, IL. GISAXS data acquisition was performed with

a 2D CCD detector (Bruker) with a resolution of $0.16 \times 0.16 \text{ mm}^2$ pixel size, fixed at a distance of 39.1 cm from the sample.

3. Results and discussion

3.1. Membrane morphology and structure

Scanning electron microscopy observations of the ceramic support surface and cross-section after aerosol deposition revealed the presence of continuous, smooth silica membrane layers of thickness $\sim 1 \text{ }\mu\text{m}$ and morphology distinctly different from that of the granular coarse-pore supports, as seen in Fig. 3. The continuity of these layers was proven by gas permeation experiments before surfactant removal, as described below. The presence of these layers was also obvious by the increase of the reflectivity of the support surface due to the high smoothness of the deposited mesostructured silica layers.

Fig. 4 shows a representative selection of TEM micrographs obtained from calcined film fragments scratched off the alumina supports. First, the TEM pictures indicate the presence of a regular mesoporous structure with a low polydispersity in pore size and shape. Second, the micrographs preferentially show rectangular patterns (Fig. 4A–C), which can be interpreted as cubic arrays of mesopores with an apparent pore diameter of $\sim 20 \text{ \AA}$. Although the regions of uniform structure are quite large (Fig. 4A), different orientations of the cubic domains can be seen in one sample (Fig. 4C), as well as domains with a certain degree of disorder, as seen in a large area of the sample in Fig. 4D. Although the exact nature of the cubic mesostructure (bcc, fcc, etc.) could not be determined from TEM alone, we can exclude the possibility that the films have significant portions of a 2D hexagonal array of cylindrical pores. In some areas of the TEM micrographs layered structures are observed, which could correspond to both 2D hexagonal and cubic structures (Fig. 4C).

Regular XRD scans of thin film samples deposited on the ceramic supports did not reveal any pronounced reflections, probably due to the random orientation of the silica mesophases in the

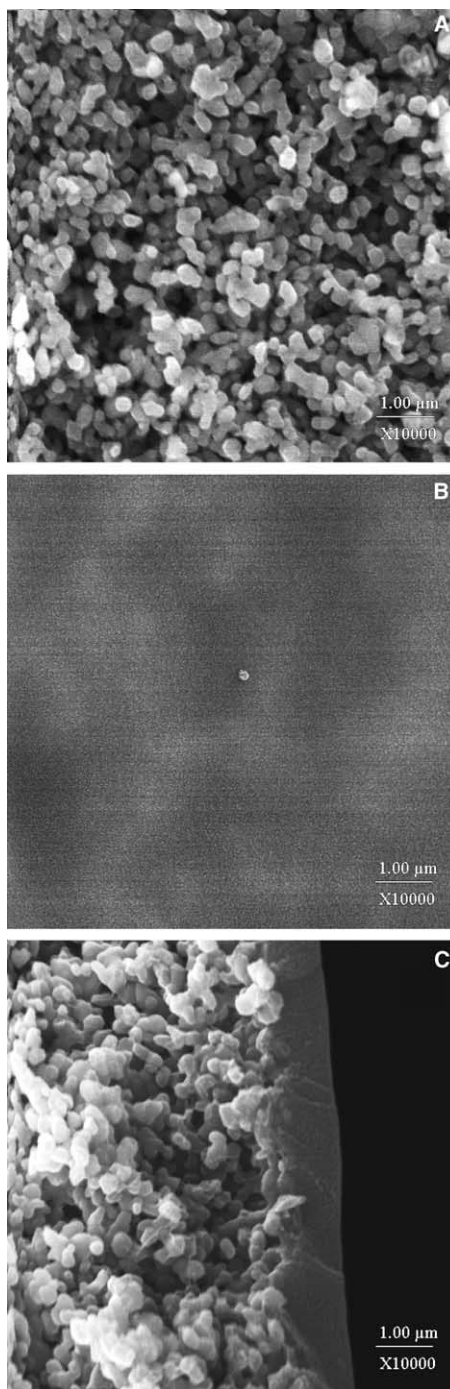


Fig. 3. SEM micrographs at a magnification of 10,000 \times of (A) surface of $\alpha\text{-Al}_2\text{O}_3$ ceramic support; (B) surface of mesoporous silica membrane; (C) cross-section of a 1- μm -thick silica membrane on the surface of the ceramic support.

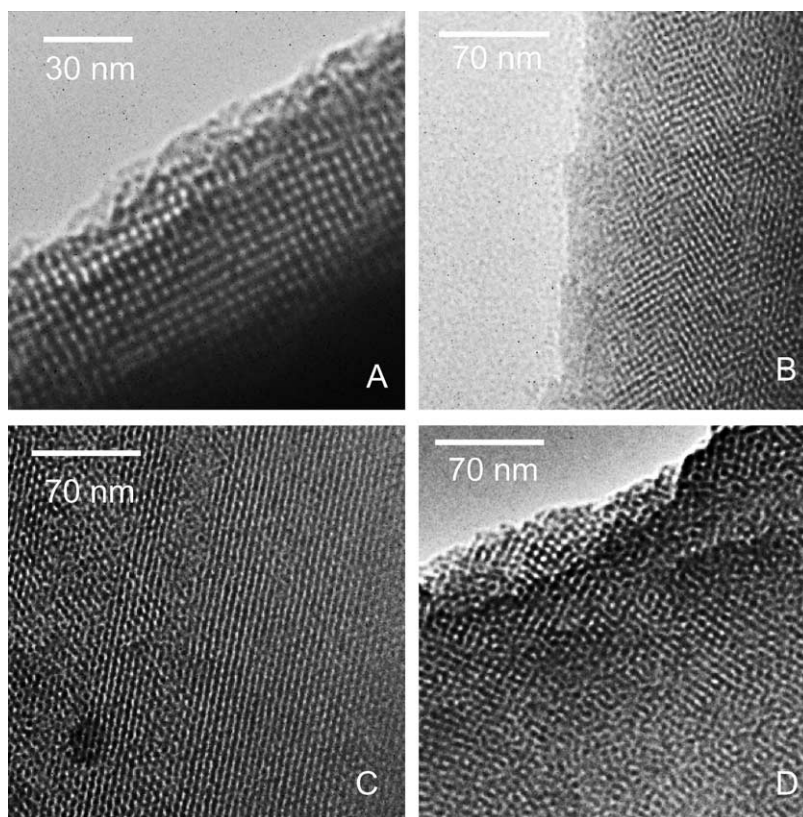


Fig. 4. TEM micrographs of calcined, cubic-ordered (A, B, C) and disordered (D) silica mesophases scratched off the ceramic support.

films, so we turned using GISAXS in order to further resolve the mesostructure of the films. GISAXS experiments with the alumina supports themselves did not show a pronounced GISAXS pattern or a significant overall GISAXS intensity, therefore their contribution to the GISAXS patterns of the coated films is almost negligible. A series of experiments under different conditions was performed, using the same surfactant-silica sol, in order to study the influence of both the support and the aerosol process on the mesostructure. Fig. 5 shows GISAXS patterns of (A) a film dip-coated on a silicon wafer; (B) a single-layer film aerosol-deposited on a Si wafer; (C) a 2-layer film aerosol-deposited on an alumina support, and (D) a 4-layer film aerosol-deposited on an alumina support.

The film dip-coated on the Si wafer (Fig. 5A) produced a GISAXS pattern with sharp, well-defined interference spots attributable to a 2D

hexagonal array of cylindrical rods. In contrast, the film sprayed onto the Si wafer showed reflections which are not in conformity with a 2D hexagonal structure, but with a cubic lattice, probably a bcc structure in $[001]$ orientation with respect to the support. A cubic structure is also in conformity with TEM results shown in Fig. 4.

The 2-layered films on the alumina supports (Fig. 5C) still show weak GISAXS reflections, indicating the presence of the cubic bcc structure, but with a certain degree of distortion or loss in orientation with respect to the support, as seen by the diffuse ring connecting the spots related to the cubic structure (the 200 reflection was so strong in intensity that it had to be shielded in order to protect the detector). Since the TEM results from these films also suggest the presence of randomly oriented cubic domains, the diffuse ring probably is mainly due to the loss in orientation with respect to the alumina support. When four layers were

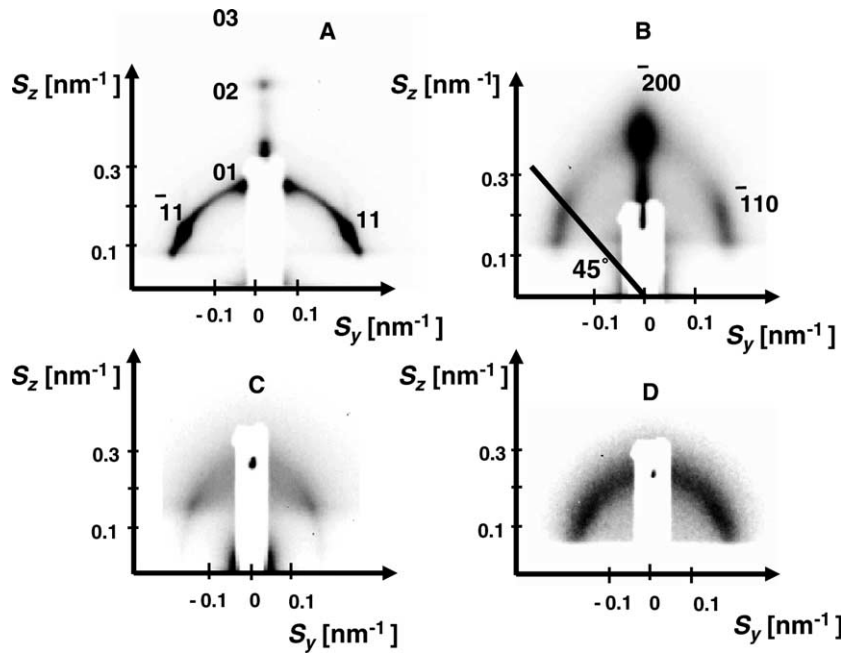


Fig. 5. GISAXS patterns of (A) a silica film deposited on a Si wafer by dip-coating; (B) a silica film aerosol-deposited on a Si wafer; (C) a 2-layer silica membrane deposited on a coarse-pore α - Al_2O_3 ceramic support; and (D) a 4-layer silica membrane deposited on a coarse-pore α - Al_2O_3 ceramic support.

deposited on the alumina support, the GISAXS patterns (Fig. 5D) were even more diffuse.

In conclusion, the GISAXS experiments reveal that the films deposited on the alumina supports or Si wafers by the aerosol method are mainly cubic-ordered, probably with a bcc structure, as opposed to 2D hexagonal mesostructures formed in films deposited on Si wafers by dip-coating. The GISAXS results are in good agreement with the TEM micrographs as regards the bcc lattice parameter of the mesostructures as well, which was estimated at ~ 50 – 55 Å. At this stage, it is suggested that the surface roughness of the alumina supports as well as the aerosol method itself may be responsible for the random orientation of the cubic mesostructures with respect to the support, as well as the presence of a certain fraction of regions with disordered pore structure or even a 2D hexagonal lattice.

3.2. Membrane permeation properties

Fig. 6A shows N_2 permeance data as a function of the pressure drop applied across the membrane,

for (1) the ceramic support, and (2) a 4-layer mesoporous silica membrane right after synthesis and drying, but before surfactant removal to empty the membrane mesopores. As seen in the figure, the N_2 permeance of the templated membrane is 4 orders of magnitude lower than that of the bare ceramic support, which suggests that complete coverage of the support surface has occurred by the overlying mesostructured surfactant/silica membrane. The permeance of other gases such as He and CH_4 relative to that of N_2 obeyed roughly the inverse relationship of the square root of the molecular weights of the test gases, suggesting that gas transport occurred through a very small number of mesoporous or even macroporous defects in the as-deposited membranes.

Fig. 6B shows N_2 permeance data as a function of the pressure drop applied across the membrane, for (1) the ceramic support, and (2) a supported, 3-layer mesoporous membrane after surfactant extraction. The permeance of the support shows a significant increase with increasing transmembrane pressure drop, consistent with contribution of

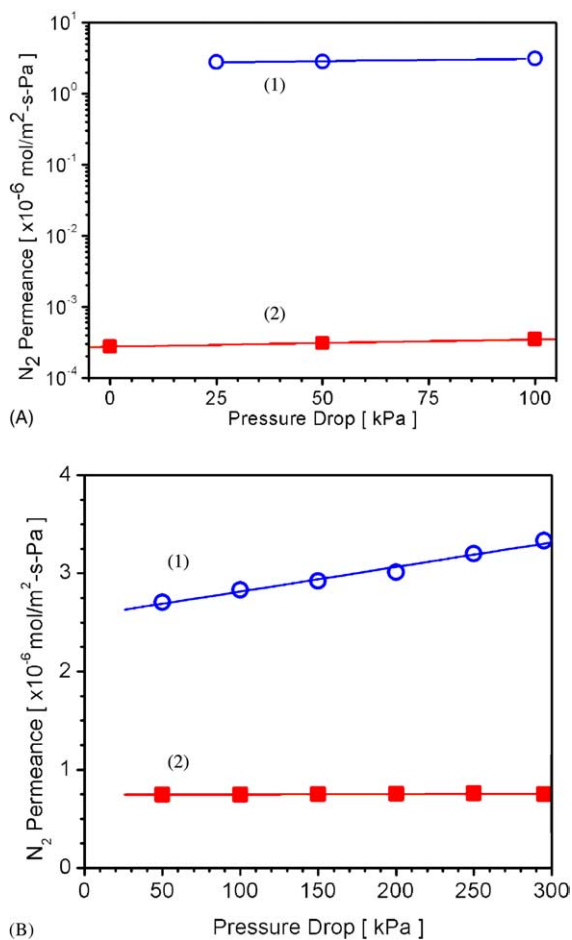


Fig. 6. (A) N₂ permeance before surfactant removal, of (1) α -Al₂O₃ ceramic support; (2) a 4-layer supported silica membrane. (B) N₂ permeance after surfactant removal, of (1) α -Al₂O₃ ceramic support; (2) a 3-layer supported silica membrane.

viscous flow through macropores which becomes important at larger feed partial pressures. On the other hand, the permeance of the supported silica membrane is practically independent of the applied pressure drop, which is consistent with Knudsen flow through small mesopores dominating the transport property of the membrane [16].

After extracting the resistance of the support assuming a resistance-in-series model for the membrane-support composite, the permeance of the silica membrane alone was estimated as $1 \times 10^{-6} \text{ mol m}^{-2} \text{ s}^{-1} \text{ Pa}^{-1}$, which is comparable to

that of a surfactant-templated silica membrane made by regular dip-coating [13]. It should be pointed out here that the effective membrane thickness may be smaller than the apparent membrane thickness determined by SEM, since the membrane layer can be asymmetric with a granular microstructure near the ceramic support/membrane interface, and truly continuous only far away from it. Nishiyama and coworkers reported a N₂ permeance of $1 \times 10^{-7} \text{ mol m}^{-2} \text{ s}^{-1} \text{ Pa}^{-1}$ for an MCM-48 silica membrane hydrothermally grown inside the pores of a $0.1 \mu\text{m}$ α -Al₂O₃ support [8], but the reason for such low permeance can be attributed to the MCM-48 material penetrating at least up to $50 \mu\text{m}$ inside the support pores.

In order to obtain more quantitative information on the distribution of pore sizes of our mesoporous silica membrane, we measured the permeance of a permanent gas, here Ar, in the presence of a condensable vapor, here ethanol, as a function of increasing relative vapor pressure, p/p_{sat} , introduced from both sides of the membrane (see Fig. 2). According to the Kelvin equation, a condensable vapor will condense in a capillary of radius r if the following equation is satisfied [17,18]:

$$RT \ln \left(\frac{p}{p_{\text{sat}}} \right) = - \frac{2\sigma v \cos \theta}{r} \quad (1)$$

where σ , v and θ are the surface tension, molar volume and contact angle, respectively. By adjusting the relative pressure of ethanol vapor in both sides of the membrane and monitoring the change in permeance of Ar, it is possible to obtain a rough estimate of the pore size distribution of the membrane.

Fig. 7 presents the results of Ar permeance as a function of (a) ethanol relative vapor pressure, and (b) as a function of corresponding Kelvin diameter, determined using Eq. (1), for a good quality, 4-layer mesoporous silica membrane (—■—), and a commercial 40 \AA γ -Al₂O₃ membrane (—○—). From a comparison of the results in Fig. 7A, it is evident that the Ar permeance of the mesoporous silica membrane decreases rapidly at low p/p_{sat} as compared to the γ -Al₂O₃ membrane, indicating that it contains mesopores, or even micropores, of size smaller than those of the respective ceramic

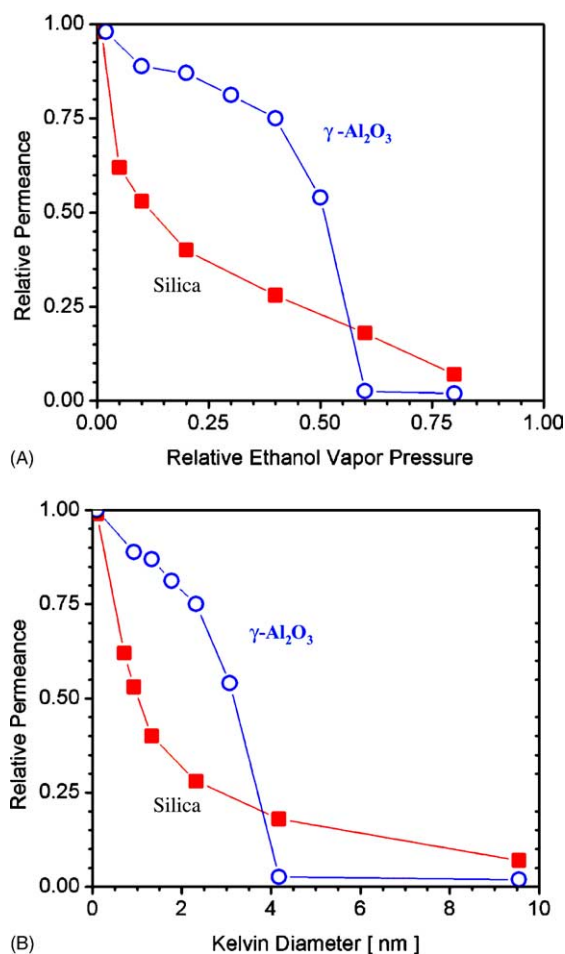


Fig. 7. Relative permeance vs. (A) relative ethanol vapor pressure and (B) Kelvin diameter, for a 4-layer mesoporous, surfactant-templated silica membrane (—■—), and a commercial 40 Å γ -Al₂O₃ membrane (—○—).

γ -Al₂O₃ membrane. By defining the average pore diameter of each membrane as the intersection of the tangent of the relative permeance curve at $P/P_0 = 0.5$ with the x -axis (Kelvin diameter) in Fig. 7B [17], we obtain ~ 20 Å for the mesoporous silica and ~ 40 Å for the commercial γ -Al₂O₃ membrane. These values are consistent with the TEM results in Fig. 4 showing mesopores of ~ 20 Å in our templated silica membranes, as well as the well known pore size of sol-gel derived γ -Al₂O₃ membrane, determined by N₂ adsorption porosimetry [4]. It is noted here that the above method can only be used for an approximate estimation of

the pore size distribution of our membranes, since the Kelvin equation is strictly valid for cylindrical pores of size larger than 20 Å, and preferably larger than 40 Å, whereas our membranes appear to consist of spherical mesopores of size closer to the lower limit of 20 Å.

It is noted here that we detected a residual Ar permeance for both membranes even for relative vapor pressure of ethanol as high as 0.8, which probably originates from diffusion of Ar through the membrane mesopores filled with liquid ethanol. Since the initial permeance of the dry γ -Al₂O₃ membrane (e.g. in the absence of ethanol) was 6–7 times higher than that of the respective silica membrane, the residual relative permeance of the latter was higher than that of the γ -Al₂O₃ membrane. In addition, for the case of the silica membranes, we cannot exclude a small contribution of N₂ permeation through the microporous silica matrix itself, which may not be entirely densified due to the low temperatures involved in the processing of the membranes, or even through larger pores or grain boundaries formed in the early stages of membrane deposition, as discussed below.

Table 1 summarizes single-component permeance data at 25 °C of a series of gases of increasing molecular weight through the same home-made 20 Å mesoporous silica and the commercial 40 Å γ -Al₂O₃ membrane samples studied in Fig. 7. If the transport mechanism responsible for permeation is Knudsen diffusion, the permeance should decrease with increasing molecular weight while the product of permeance and square root of molecular weight, $P \cdot \sqrt{M}$, should be invariable. Variations from this rule could arise when: (i) other transport mechanisms apply as well, e.g. surface diffusion; (ii) when the transport resistance of the macroporous support (α -Al₂O₃) is comparable with that of the mesoporous membrane; or (iii) when the mesoporous membrane is defective.

For the case of the γ -Al₂O₃ membrane, the permeance decreases with increasing M of the probe gases, and the product $P \cdot \sqrt{M}$ is nearly the same for CH₄, N₂, Ar and CO₂. The variations observed for He and SF₆ could be a result of increasing importance of support resistance or contribution from surface flow, respectively. For the

Table 1

Single-component permeance at 25 °C of a series of gases of increasing molecular weight through a 20 Å 4-layer mesoporous silica and a commercial 40 Å γ -Al₂O₃ membrane

Membrane	Permeance [$\times 10^{-7}$ mol m ⁻² s ⁻¹ Pa ⁻¹] (permeance $\times \sqrt{M}$)					
	He (4)	CH ₄ (16)	N ₂ (28)	Ar (40)	CO ₂ (44)	SF ₆ (146)
20 Å Silica	6.74 (13.5)	3.74 (15.0)	2.77 (14.7)	2.37 (15.0)	3.42 (22.7)	1.48 (17.9)
40 Å γ -Al ₂ O ₃	40.7 (81.4)	25.4 (101.6)	19.3 (102.1)	15.6 (98.7)	15.2 (100.8)	10.7 (129.3)

case of the mesoporous silica membrane, we observe that $P \cdot \sqrt{M}$ is nearly the same within 10% for He, CH₄, N₂ and Ar but is higher for CO₂ and SF₆. More strikingly, the permeance of CO₂ is higher than that of N₂ and Ar, which suggests significant contribution of surface flow, or even transport through micropores interconnecting the mesopores of the membrane. This effect together with its lower permeance compared to the γ -Al₂O₃ membrane, is further evidence that transport through our mesoporous silica membranes is controlled by pores of size smaller than the 40 Å pores of the γ -Al₂O₃ membrane.

At this point, it is safe to state that the combined SEM, TEM, GISAXS and gas permeation data indicate that our silica membranes are composed of randomly oriented, cubic-ordered mesoporous domains with pores of size ~ 20 Å, giving rise to substantial transmembrane permeance and probably isotropic flow characteristics, although we cannot exclude the presence of a small population of pores with size >40 Å, as manifested by the permporosimetry data shown in Fig. 7. These larger pores are more likely grain boundaries between neighboring granular or particulate silica deposits formed on the ceramic support at the early stages of membrane deposition, which apparently were not covered up entirely during subsequent deposition of silica material at the later stages of the deposition process.

4. Conclusions

We have demonstrated a novel, aerosol-assisted deposition technique for rapid formation of surfactant-templated mesoporous silica membranes on coarse-pore ceramic supports. This method could prove valuable for development of a new genera-

tion of ultrafiltration inorganic membranes on inexpensive ceramic or metallic supports, as an alternative to well-known nanocrystalline ultrafiltration ceramic membranes, e.g. γ -Al₂O₃, TiO₂ and ZrO₂. The advantages of the new membranes include simple synthesis chemistry, narrow pore size distribution, high thermal and structural stability and finally, tunability of the pore wall chemistry to expand the separation potential of these membranes.

Acknowledgements

We would like to acknowledge financial support from Pall Corporation, PPG Industries, NASA, the UNM/NSF Center for Microengineered Materials and the DOE Basic Energy Sciences Program. We are indebted to Dr. Alan J. Hurd for many useful technical discussions during the course of this project. We would also like to thank the Advanced Photon Source at the Argonne National Laboratory for allocating time for the GISAXS experiments, as well as Dr. Jin Wang for his assistance in the beam measurements. Use of the Advanced Photon Source was supported by DOE Office of Science and Office of Basic Energy Sciences, under contract W-31-109-Eng-38. Sandia is a multiprogram laboratory operated by Sandia Corporation, a Lockheed Martin Company, for the US Department of Energy under contract DE-AC04-94AL85000.

References

- [1] R. Bhave, *Inorganic Membranes: Synthesis, Characterization and Applications*, Van Nostrand Reinhold, New York, 1991.

- [2] C.J. Brinker, R. Sehgal, S.L. Hietala, R. Deshpande, D.M. Smith, D. Loy, C.S. Ashley, Sol-gel strategies for controlled porosity inorganic materials, *J. Membr. Sci.* 94 (1994) 85.
- [3] A.J. Burggraaf, L. Cot (Eds.), *Fundamentals of Inorganic Membrane Science and Technology*, Membrane Science and Technology Series, vol. 4, Elsevier, Amsterdam, 1996, Chapter 1.
- [4] C.H. Chang, R. Gopalan, Y.S. Lin, A comparative study on thermal and hydrothermal stability of alumina, titania and zirconia membranes, *J. Membr. Sci.* 91 (1994) 27.
- [5] C.T. Kresge, M.E. Leonowicz, W.J. Roth, J.C. Vartuli, J.S. Beck, Ordered mesoporous molecular sieves synthesized by a liquid-crystal template mechanism, *Nature* 359 (1992) 710.
- [6] M. Ogawa, N. Masukawa, Preparation of transparent thin films of lamellar, hexagonal and cubic silica-surfactant mesostructured materials by rapid solvent evaporation methods, *Microp. Mesop. Mater.* 38 (2000) 35.
- [7] N. Nishiyama, A. Koide, Y. Egashira, K. Ueyama, Mesoporous MCM-48 membrane synthesized on a porous stainless steel support, *Chem. Commun.* (1998) 2147.
- [8] N. Nishiyama, D.H. Park, A. Koide, Y. Egashira, K. Ueyama, A mesoporous silica (MCM-48) membrane: preparation and characterization, *J. Membr. Sci.* 182 (2001) 235.
- [9] N. Nishiyama, D.H. Park, Y. Egashira, K. Ueyama, Pore size distributions of silylated mesoporous silica MCM-48 membranes, *Separ. Purif. Technol.* 32 (2003) 127.
- [10] H.W. Hillhouse, T. Okubo, J.W. van Egmond, M. Tsapatsis, Preparation of supported mesoporous silica layers in a continuous flow cell, *Chem. Mater.* 9 (1997) 1505.
- [11] Y. Lu, R. Ganguli, C.A. Drewien, M.T. Anderson, C.J. Brinker, W. Gong, Y. Guo, H. Soyez, B. Dunn, M.H. Huang, J.I. Zink, Continuous formation of supported cubic and hexagonal mesoporous films by sol-gel dip-coating, *Nature* 389 (1997) 364.
- [12] C.Y. Tsai, S.Y. Tam, Y. Lu, C.J. Brinker, Dual-layer asymmetric microporous silica membranes, *J. Membr. Sci.* 169 (2000) 255.
- [13] G. Xomeritakis, S. Naik, C.M. Braunbarth, C.J. Cornelius, R. Pardey, C.J. Brinker, Organic-templated silica membranes I. Gas and vapor transport properties, *J. Membr. Sci.* 215 (2003) 225.
- [14] Z. Lai, G. Bonilla, I. Diaz, J.G. Nery, K. Sujaoti, M.A. Amat, E. Kokkoli, O. Terasaki, R.W. Thompson, M. Tsapatsis, D.G. Vlachos, Microstructural optimization of a zeolite membrane for organic vapor separation, *Science* 300 (2003) 456.
- [15] www.baikowski.com.
- [16] Y.S. Lin, A.J. Burggraaf, Preparation and characterization of high-temperature thermally stable alumina composite membrane, *J. Am. Ceram. Soc.* 74 (1991) 219.
- [17] T. Tsuru, T. Hino, T. Yoshioka, M. Asaeda, Permporometry characterization of microporous ceramic membranes, *J. Membr. Sci.* 186 (2001) 257.
- [18] T. Tsuru, Y. Takata, H. Kondo, F. Hirano, T. Yoshioka, M. Asaeda, Characterization of sol-gel derived membranes and zeolite membranes by nanoporometry, *Separ. Purif. Technol.* 32 (2003) 23.